

## Properties of the Coolest Dwarfs

S. Leggett<sup>1</sup>, R. Freedman<sup>2</sup>, T. Geballe<sup>1</sup>, D. Golimowski<sup>3</sup>, N. Lodieu<sup>4</sup>,  
M. Marley<sup>5</sup>, D. Pinfield<sup>6</sup>, D. Saumon<sup>7</sup>, D. Stephens<sup>8</sup>, S. Warren<sup>9</sup>

**Abstract.** Eleven years after the discovery of the first T dwarf, a population of ultracool L and T dwarfs has been identified that is large enough to show a range of atmospheric properties. Also, model atmospheres are sufficiently advanced to study these properties in detail. Since the last Cool Stars meeting, several observational developments have aided in these studies. We present recent mid-infrared photometry and spectroscopy from the *Spitzer Space Telescope* which confirms the prevalence of vertical mixing in the atmospheres of L and T dwarfs. Hence, the 700 K to 2200 K L and T dwarf photospheres require several parameters for successful modelling: effective temperature, gravity, metallicity, grain sedimentation efficiency and vertical mixing efficiency. We also describe initial results of a search for ultracool dwarfs in the UKIRT Infrared Deep Sky Survey, and present the latest T dwarf found to date. We conclude with a discussion of the possible spectral indicators of Y dwarfs.

### 1. Introduction

The first L dwarf and T dwarf were discovered as companions to nearby objects by Becklin & Zuckerman in 1988 and by Nakajima et al. in 1995, respectively. After several more years other examples were revealed, primarily as a result of sky surveys: the red-sensitive SDSS Sloan Digital Sky Survey (SDSS; York et al. 2000) and the near-infrared Two Micron All Sky Survey (2MASS; Skrutskie et al. 2006). There are now  $\sim$ 500 confirmed L dwarfs and  $\sim$ 100 confirmed T dwarfs, and the sample is large enough to enable detailed studies of physical parameters such as effective temperature ( $T_{\text{eff}}$ ), gravity and metallicity.

Since Cool Stars 13 there have been many observational developments in studies of cool brown dwarfs. One of these is Laser Guide Star Adaptive Optics

---

<sup>1</sup>Gemini North, 670 N. A'ohoku Place, Hilo, HI 96720, USA

<sup>2</sup>SETI, MS 245-3, NASA Ames Research Center, Moffett Field, CA 94035, USA

<sup>3</sup>Phys. & Astr., Johns Hopkins University, 3400 N. Charles St., Baltimore, MD 21218, USA

<sup>4</sup>Instituto de Astrofisica de Canarias, Via Lactea, E38205 La Laguna, Tenerife, Spain

<sup>5</sup>MS 245-3, NASA Ames Research Center, Moffett Field, CA 94035, USA

<sup>6</sup>Science & Technology Inst., University of Hertfordshire, Hatfield, Herts AL10 9AB, UK

<sup>7</sup>Los Alamos National Laboratory, MS P365, Los Alamos, NM 87545, USA

<sup>8</sup>Brigham Young University, Dept. of Physics & Astronomy, N145 ESC, Provo, UT 84602, USA

<sup>9</sup>Astrophysics, Imperial College, Blackett Lab., Prince Consort Road, London SW7 2AZ, UK

discussed in the “Sub-Stellar Twins” splinter session, and other contributions to these proceedings. Here we describe two other advances: the UKIRT Infrared Deep Sky Survey (UKIDSS), which goes  $\sim 3$  magnitudes deeper than 2MASS; and the mid-infrared capabilities of the *Spitzer Space Telescope*, which offers large sensitivity enhancements in the 3–160  $\mu\text{m}$  wavelength region.

## 2. 3–14 $\mu\text{m}$ Spectra and 3–9 $\mu\text{m}$ Colors of L and T Dwarfs

### 2.1. Modelling the Photospheres of L and T Dwarfs

We have found that five parameters are required for successful modelling of L and T dwarf atmospheres. Three of these will be familiar to stellar astronomers —  $T_{\text{eff}}$ , surface gravity ( $\log g$ ), and metallicity ([m/H]). The other two factors are more usually associated with planetary atmospheres — grain sedimentation, which we describe by a sedimentation efficiency  $f_{\text{sed}}$ , and vertical mixing, which we describe by a diffusion coefficient  $K_{zz}$ . In the following we explore the effect of these parameters on *Spitzer* mid-infrared data. Van Gordon et al. (these proceedings) discuss variable water and silicate features in 5–15  $\mu\text{m}$  spectra.

### 2.2. Effective Temperatures of L and T Dwarfs

The most fundamental of the photospheric parameters is  $T_{\text{eff}}$ . The most accurate determination of  $T_{\text{eff}}$  uses the observed bolometric luminosity at the Earth, for those dwarfs with known distance. The radii of brown dwarfs older than 200 Myr, with masses 0.3–70  $M_{\text{Jupiter}}$ , are within 30% of  $R_{\text{Jupiter}}$  (e.g. Figure 10 of Burrows et al. 1997). Hence luminosity is nearly proportional to  $T_{\text{eff}}^4$  and  $T_{\text{eff}}$  can be very accurately determined from the luminosity. Saumon et al. (2006, 2007) show how, with not very rigorous age constraints derived from main sequence primaries or from kinematics, luminosity determines  $T_{\text{eff}}$  to  $\leq \pm 50$  K, for the coolest T dwarfs with  $750 \leq T_{\text{eff}} \leq 900$  K. Comparison to synthetic spectra allows gravity to be constrained, which allows mass to be determined and allows age to be further constrained, for cooling brown dwarfs.

Figure 1 plots spectral type against  $T_{\text{eff}}$ , where  $T_{\text{eff}}$  has been derived from luminosity. This is an updated version of Figure 6 in Goliowski et al. (2004a):  $T_{\text{eff}}$  is adjusted for recently discovered multiple systems (Burgasser et al. 2005, 2006b; Goliowski et al. 2004b, Liu & Leggett 2005), and the new results of Saumon et al. (2006, 2007) and Luhman et al. (2007) are included.

### 2.3. Vertical Mixing Diffusion Coefficient

The mid-infrared spectra of T dwarfs are more sensitive to  $K_{zz}$  than to  $\log g$ , [m/H] or  $f_{\text{sed}}$ . For both L and T dwarfs, turbulent vertical mixing draws up long-lived chemical species from deep, hot layers into the cool radiative photosphere, so that these species are over-abundant. In the models  $K_{zz} \text{ cm}^2\text{s}^{-1}$  is treated as a tunable parameter in the nominally stable radiative zone. The abundances of species like CO and N<sub>2</sub> are enhanced in the upper atmosphere, while those of H<sub>2</sub>O, CH<sub>4</sub> and NH<sub>3</sub> are reduced (e.g. Saumon et al. 2007 and references therein). Non-equilibrium chemistry has a profound effect at mid-infrared wavelengths as the abundances of CO and NH<sub>3</sub> can be altered by more than an order of magnitude (e.g. Figure 3 of Saumon et al. 2006), and these species have strong

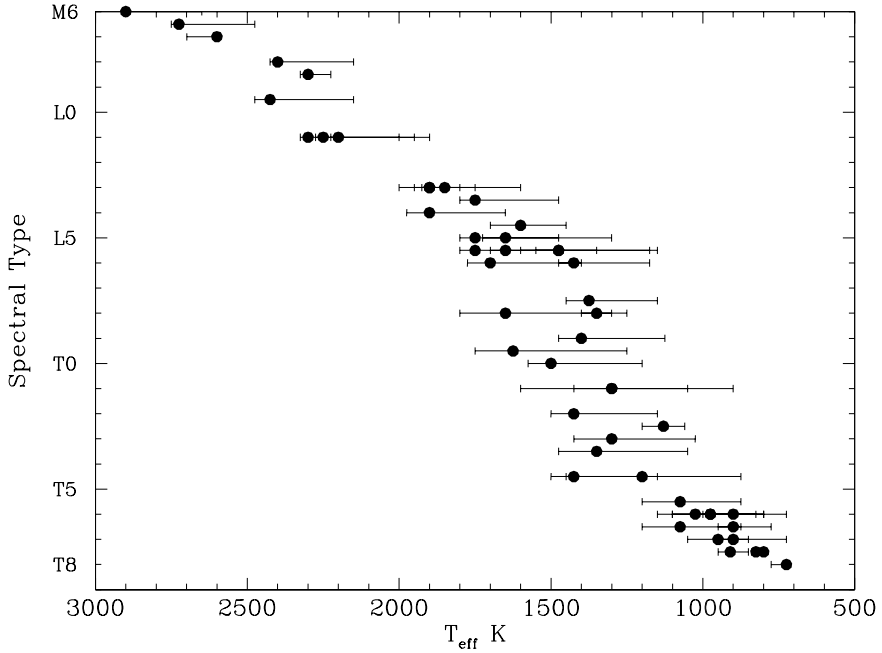


Figure 1. Spectral type (based on the infrared classification schemes of Geballe et al. 2002 and Burgasser et al. 2006a) against  $T_{\text{eff}}$ . Error bars reflect the unknown ages of the dwarfs; for most objects an age range of 0.1–10 Gyr is allowed; the solid symbol indicates  $T_{\text{eff}}$  at 3 Gyr.

features at  $5 \mu\text{m}$  and  $10 \mu\text{m}$ . The mixing is not important for T dwarfs in the near-infrared however as the abundances of the species with dominant opacities there,  $\text{H}_2\text{O}$  and  $\text{CH}_4$ , are not significantly affected. For late-L dwarfs the changes to the CO and  $\text{CH}_4$  abundances do impact the  $2 \mu\text{m}$  spectral region.

Figure 2 demonstrates the impact of vertical mixing on mid-infrared spectra of a late-L and a late-T dwarf. Figure 6 of Leggett et al. (2007) shows that the mixing also significantly affects ground-based  $K - L'$  and  $L' - M$  colors, as well as the *Spitzer* IRAC colors [3.55]–[4.49] and [4.49]–[5.73]. As Figure 2 shows, with the onset of this mixing, the  $3.3 \mu\text{m}$  and  $8.0 \mu\text{m}$   $\text{CH}_4$  absorption bands in L dwarfs weaken, the  $4.8 \mu\text{m}$  CO absorption band in both L and T dwarfs strengthens, and the  $9$ – $13 \mu\text{m}$   $\text{NH}_3$  absorption band in T dwarfs weakens. Hence  $K - L'$  becomes redder,  $L' - M$  and [3.55]–[4.49] bluer, and [4.49]–[5.73] redder. The best match to the IRAC colors indicates  $K_{zz} \approx 10^4 \text{ cm}^2\text{s}^{-1}$ .

## 2.4. Grain Sedimentation and Metallicity

At temperatures  $\sim 1500 \text{ K}$ , iron and silicate grains condense. Cloud decks containing these grains lie within the photospheres of the L dwarfs, and below the photospheres of the cooler T dwarfs. Hence for T dwarfs the condensation only impacts the spectral energy distribution (SED) by reducing the abundances of

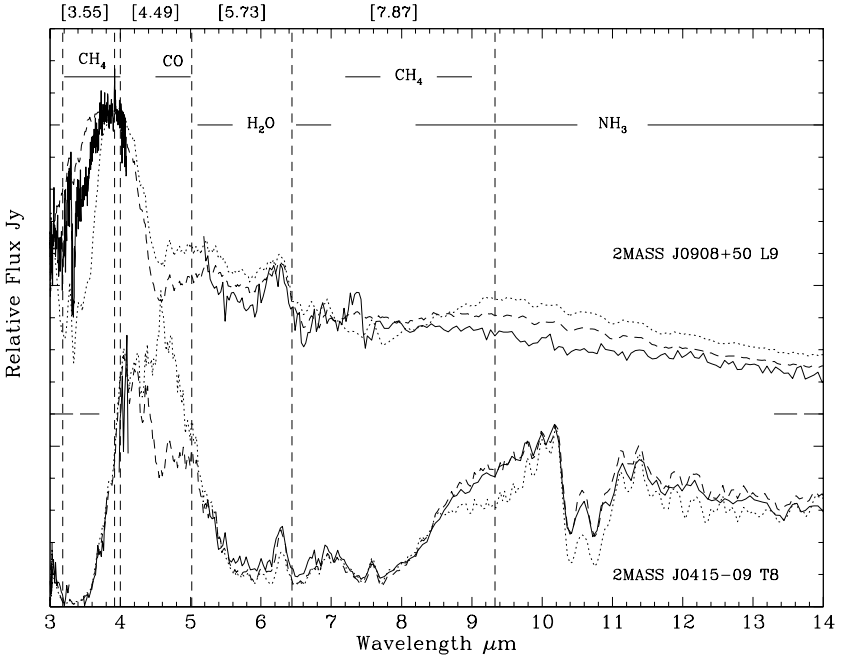


Figure 2. Observed 3–14  $\mu\text{m}$  spectra (black curves) for the late L dwarf 2MASS J0908+50 (Stephens et al. in prep.) and the late T dwarf 2MASS J0415-09 (Saumon et al. 2007) are shown; the L dwarf is offset for clarity, dashed lines indicate its zero flux level. Synthetic spectra with  $\log g = 5.0$  and  $[\text{m}/\text{H}] = 0$  are also shown; for the L9 these have  $T_{\text{eff}} = 1400$  K and  $f_{\text{sed}} = 2$  with  $K_{zz} = 0$  (dotted) and  $K_{zz} = 10^4$  (dashed), for the T8  $T_{\text{eff}} = 700$  K cloudless spectra with  $K_{zz} = 0$  (dotted) and  $K_{zz} = 10^4$  (dashed) are shown. The four IRAC bandpasses, and principal absorbing species, are indicated.

O, Fe, Si, Mg, Ti, and other refractory species. The models by Marley and colleagues include cloud decks of condensates whose vertical extents are determined by the balance between upward turbulent mixing and downward sedimentation. A parameter  $f_{\text{sed}}$  measures the ratio of sedimentation to convection velocities (Ackerman & Marley 2001): high  $f_{\text{sed}}$  means efficient sedimentation and thin cloud decks, and vice versa. For Jupiter's  $\text{NH}_3$  clouds  $f_{\text{sed}} \sim 2$ .

Figure 3 shows synthetic mid-infrared spectra with different values of  $f_{\text{sed}}$ . Varying  $f_{\text{sed}}$  does not impact the SEDs of late T dwarfs as expected. For L dwarfs, increasing  $f_{\text{sed}}$  from 2 to 3 decreases the 3–14  $\mu\text{m}$  flux by  $\sim 20\%$ . The Leggett et al. (2007, their Figure 5) study of IRAC L and T dwarf colors shows effects of similar size, although adopting  $f_{\text{sed}} = 1$  produces larger changes in all bands. Leggett et al. show that L and early-T dwarfs with unusual near-infrared colors also have unusual IRAC colors. Abnormally infrared-blue or -red dwarfs seem to require abnormally thin or thick cloud decks, respectively, but the effects of metallicity on the L dwarf cloud decks are yet to be explored.

Non-solar metallicity models are available for T dwarfs, and Figure 3 shows that reducing  $[m/H]$  by 0.3 dex does not significantly impact the mid-infrared SED of late-T dwarfs. Leggett et al. (2007, Figure 5) arrive at similar conclusions — while metallicity is very important at  $2\mu\text{m}$ , it is not significant at longer wavelengths. Note in Figure 3 that changing  $f_{\text{sed}}$  for the L dwarf, or metallicity for the T dwarf, does not improve the poor match to the  $\text{CH}_4$  and  $\text{NH}_3$  features — this improvement is only achieved by introducing vertical mixing (Figure 2).

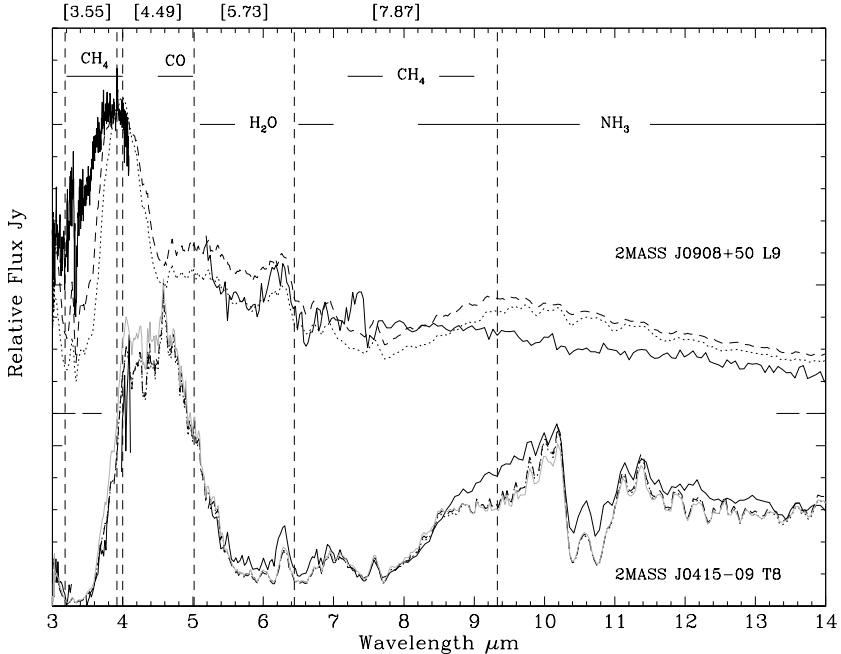


Figure 3. Similar to Figure 2 but here synthetic spectra with  $K_{zz} = 0$ ,  $\log g = 5.0$  and  $[m/H] = 0$  are shown with  $T_{\text{eff}} = 1400\text{ K}$  (top)  $f_{\text{sed}} = 2$  (dash) and  $f_{\text{sed}} = 3$  (dot);  $T_{\text{eff}} = 700\text{ K}$  (bottom) cloudless (dash) and  $f_{\text{sed}} = 3$  (dot). Also in grey is a cloudless 700 K  $[m/H] = -0.3$  spectrum.

## 2.5. Gravity

Figure 4 shows synthetic spectra for different values of surface gravity. A 0.5 dex change in gravity does not significantly impact the mid-infrared SED: only a  $\sim 10\%$  change in the  $4\mu\text{m}$  flux is seen. The Leggett et al. (2007, Figure 4) study of L and T dwarf IRAC colors arrives at similar conclusions — while gravity is very important at  $2\mu\text{m}$ , it is not significant at longer wavelengths, except that the  $[4.49] - [5.73]$  color of T dwarfs becomes bluer with increasing gravity. Note in Figure 4 that changing gravity for the L or T dwarfs does not improve the poor match to the  $\text{CH}_4$  and  $\text{NH}_3$  features — this improvement is only achieved by introducing vertical mixing (Figure 2).

### 3. Mid-Infrared Magnitudes, Colors and Temperature Indicators

#### 3.1. Color-Magnitude Diagrams

Although gravity has little effect on mid-infrared colors, it does affect the absolute fluxes as gravity is nearly proportional to mass and hence luminosity. Patten et al. (2006) suggest that the spread seen for the T dwarfs in IRAC color-magnitude diagrams reflects the range in gravity (or mass) in the sample.

Figure 5 plots color-magnitude diagrams for the three shorter-wavelength IRAC bandpasses. For T dwarfs, the sequences demonstrate the effects of changing  $K_{zz}$  from 0 to  $10^4 \text{ cm}^2 \text{s}^{-1}$ ,  $\log g$  from 4.5 to 5.5 and  $[\text{m}/\text{H}]$  from  $-0.3$  to  $+0.3$ . These values of  $g$  and  $[\text{m}/\text{H}]$  are appropriate for field T dwarfs (e.g. Burrows et al. 1997). The plot shows that gravity cannot explain the spread in the T dwarf sequence in  $M_{[4.49]}:[4.49]-[5.73]$  although the large range in metallicity of 0.6 dex could. The 1.0 dex range in gravity and/or 0.6 dex range in metallicity could approximately cover the observed spread in the  $M_{[3.55]}:[3.55]-[4.49]$  plot.

However, Figure 5 shows that varying  $K_{zz}$  produces a large change in the location of the sequences, and furthermore that  $K_{zz} \sim 10^4 \text{ cm}^2 \text{s}^{-1}$  is required to reproduce the observational data. It is possible that the spread in the sequences reflects a range in the vertical mixing diffusion coefficient for T dwarfs. Until

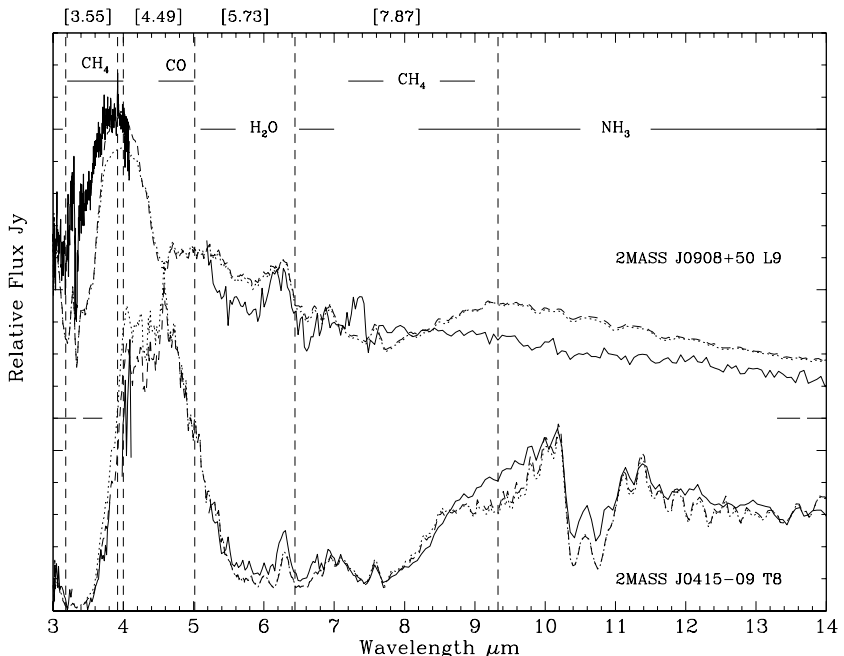


Figure 4. Similar to Figures 2 and 3; synthetic spectra with  $K_{zz} = 0$  and  $[\text{m}/\text{H}] = 0$  are shown with  $T_{\text{eff}} = 1400 \text{ K}$ ,  $f_{\text{sed}} = 2$ , (top) and  $T_{\text{eff}} = 700 \text{ K}$ , cloudless (bottom). Dashed curves have  $\log g = 5.0$  and dotted  $\log g = 5.5$ .

a full hydrodynamic model is available which incorporates both the condensate cloud decks and chemical dredge-up, the absolute values and range of  $K_{zz}$  cannot be accurately known. If this parameter lies in the range  $10^2 \lesssim K_{zz} \lesssim 10^6 \text{ cm}^2\text{s}^{-1}$ , then the mixing timescales in the photosphere are  $\sim 10$  years to 1 hour.

### 3.2. Temperature Indicators

Figure 6 plots  $K - L'$  and  $[3.55] - [4.49]$  as a function of  $T_{\text{eff}}$  (see §2.2).  $K - L'$  can be a useful temperature indicator for young obscured low-mass objects, or for L dwarfs, as these wavelengths are less sensitive than  $J$  and  $H$  to the silicate clouds. However Figure 6 shows that for T dwarfs, while  $K - L'$  is not significantly affected by vertical mixing, it is very sensitive to both gravity and metallicity, due to strong pressure-induced H<sub>2</sub> opacity at 2  $\mu\text{m}$ . For a given value of  $K - L'$  an uncertainty in gravity of  $\pm 0.5$  dex or in metallicity of  $\pm 0.3$  dex leads to an uncertainty in implied  $T_{\text{eff}}$  of  $\sim \pm 150$  K, for objects cooler than  $\sim 1100$  K.

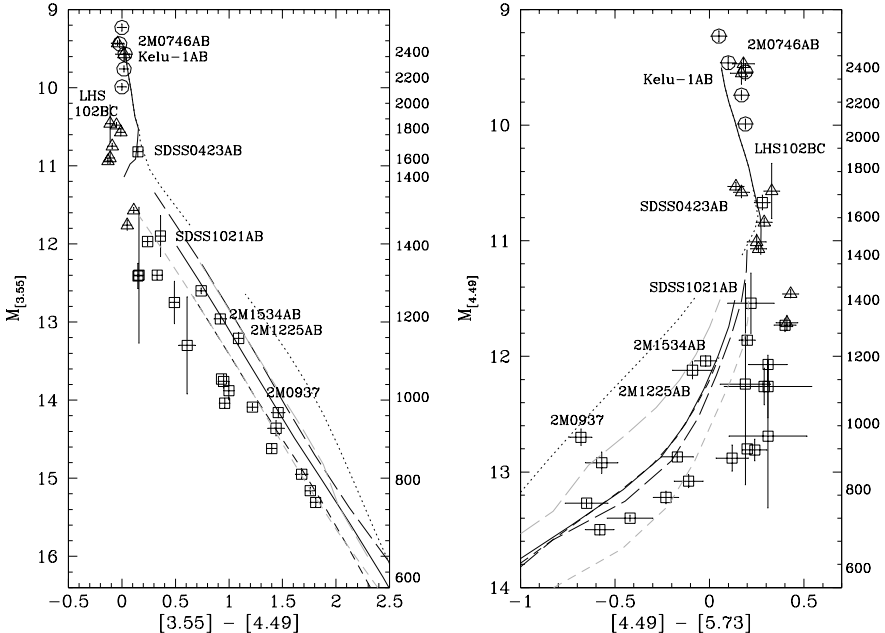


Figure 5. Color-magnitude diagrams for M (circles), L (triangles) and T dwarfs (squares; Patten et al. 2006, Leggett et al. 2007, Luhman et al. 2007). Known binaries are identified. Sequences are models; dotted have  $K_{zz} = 0$ , others  $K_{zz} = 10^4$ . Upper solid and dotted curves have  $[m/H] = 0$ ,  $f_{\text{sed}} = 2$  and  $\log g = 5.0$ , the  $1400 \leq T_{\text{eff}} \text{ K} \leq 2400$  values for  $K_{zz} = 10^4$  are shown at top right. Lower curves are cloudless. The solid curve has  $[m/H] = 0$ ,  $\log g = 5.0$ , and the  $600 \leq T_{\text{eff}} \text{ K} \leq 1400$  values for  $K_{zz} = 10^4$  are shown at bottom right. Black short-dash curves have  $\log g = 5.5$  and long-dashed  $\log g = 4.5$ . Grey short-dash curves have  $[m/H] = +0.3$  and long-dashed  $[m/H] = -0.3$ .

Leggett et al. (2007) suggest that the IRAC [3.55]–[4.49] color is a useful temperature indicator for extremely cool dwarfs, as it is insensitive to  $f_{\text{sed}}$ ,  $\log g$  and [m/H]. Figure 6 shows however that this color is sensitive to  $K_{zz}$ . If  $\log K_{zz}$  varies between dwarfs by as much as  $\pm 2$ , then an uncertainty of  $\sim \pm 100$  K is implied. Note that Figures 2, 5 and 6 indicate that  $K_{zz} \sim 10^4 - 10^6 \text{ cm}^2 \text{s}^{-1}$  is necessary to reproduce the various observational data, and we believe a variation in  $\log K_{zz}$  as high as  $\pm 2$  is unlikely.

Both  $K - L'$  and [3.55]–[4.49] continue to increase at very low temperatures, as does  $K - [3.55]$ , making these colors promising for confirming extreme-T, or the even later type Y, dwarfs. These objects will be faint however, and ground-based observations, especially at  $L'$ , will be challenging. The mid-infrared sensitivity of *Spitzer* (or subsequent space missions) makes [3.55]–[4.49] (or similar colors) a more practical temperature indicator for such objects than  $K - L'$ .

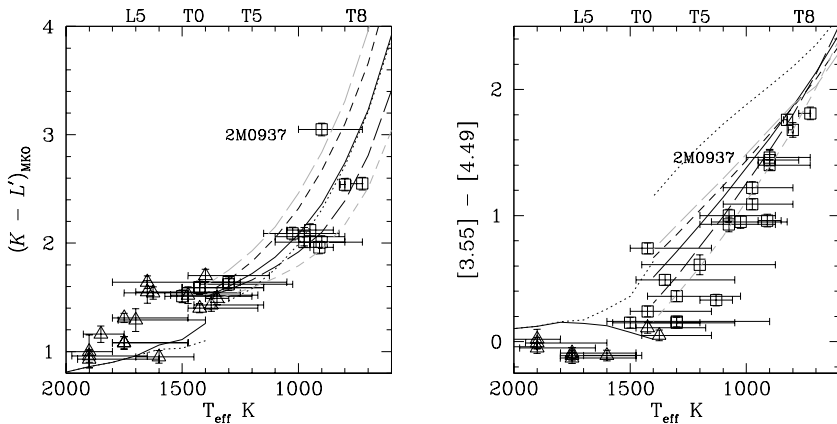


Figure 6. Observed  $K - L'$  and [3.55]–[4.49] colors as a function of  $T_{\text{eff}}$ . Symbols and line types are as in Figure 5. Approximate spectral types are indicated and the peculiar T dwarf 2MASSJ0937+29 is identified.

#### 4. The Search for Extreme-T or Y Dwarfs

##### 4.1. The UKIRT Infrared Deep Sky Survey

The splinter session ‘‘Mining the Next Generation of Surveys for Cool Star Science’’ describes surveys sensitive to very cool brown dwarfs (see also Delorme et

al., these proceedings). Here we describe one such survey, the UKIRT Infrared Deep Sky Survey (UKIDSS), and the results of a T and Y dwarf search in the first, recently released, UKIDSS data.

UKIDSS started operation in May 2005 and is projected to take seven years. The survey is described by Lawrence et al. (2007), and the photometric systems and colors of various sources by Hewett et al. (2006). The survey consists of five sub-surveys: the Large Area Survey (LAS), Galactic Plane Survey (GPS), Galactic Clusters Survey (GCS), Deep Extragalactic Survey (DXS) and Ultra Deep Survey (UDS). Of these, the LAS is designed to target cool brown dwarfs. It will cover  $4000 \text{ deg}^2$  in  $YJHK$  filters ( $\lambda_{\text{eff}}$  1.03, 1.25, 1.63 and  $2.20 \mu\text{m}$ ) to a depth of  $Y = 20.3$ ,  $J = 19.9$ ,  $H = 18.6$  and  $K = 18.2$ . Figure 7 shows that T and Y dwarfs should be identifiable by their red  $Y - J$  and blue  $J - H$  colors.  $K$  will be extremely faint as  $H - K$  is also blue. Models (e.g. Burrows et al. 2003) suggest that the LAS will be sensitive at  $YJH$  to dwarfs with  $T_{\text{eff}} = 500 \text{ K}$  at 10pc, or equivalently a 1 Gyr old  $10 M_{\text{Jupiter}}$  mass object at 10pc.

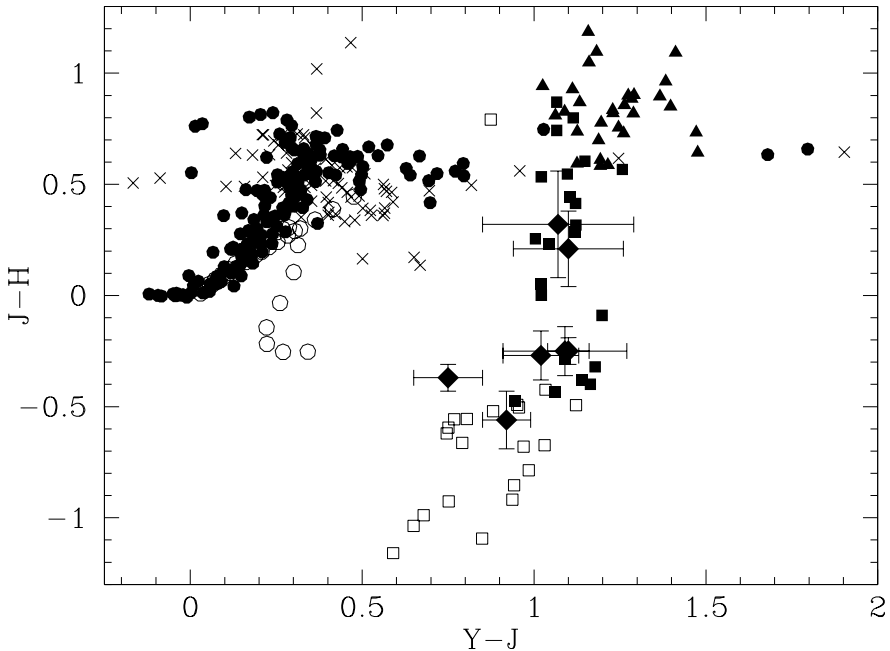


Figure 7. Synthesized  $YJH$  colors from observed spectra are solid symbols: A–M stars – circles, L dwarfs – triangles, T dwarfs – squares. The colors of the new UKIDSS T dwarfs are diamonds. Model colors of quasars (crosses), white dwarfs (open circles), and  $T_{\text{eff}} = 550\text{--}900 \text{ K}$  T/Y dwarfs (open squares) are also shown. From Hewett et al. (2006), Allard & Homeier (priv. comm.).

## 4.2. First Results from UKIDSS

There have been two UKIDSS data releases: the Early Data Release in February 2006 (EDR, Dye et al. 2006) and Data Release 1 in July 2006 (DR1, Warren et al. 2007). The EDR covers  $29 \text{ deg}^2$ , and DR1  $190 \text{ deg}^2$ , of the LAS. The UKIDSS Cool Dwarf Group has followed up candidates in a  $\sim 150 \text{ deg}^2$  area. Four T5.0–T5.5 and two T7.5–T8.5 dwarfs have been spectroscopically confirmed, and another  $\sim \text{T5}$  confirmed by CH<sub>4</sub> imaging (Figure 7; Kendall et al. 2007; Lodieu et al., Warren et al. in prep.). Distance estimates are  $\sim 20\text{--}70 \text{ pc}$ .

Deacon & Hambly (2006) simulated the UKIDSS T and Y dwarf detections for various mass functions and star formation rates. The initial detections are consistent with a flat or slightly increasing mass function, and suggest UKIDSS will find around 100 dwarfs later than T8 over the course of the survey.

## 4.3. ULAS J0034 — the Coolest Brown Dwarf

Figure 8 plots 0.95–1.70  $\mu\text{m}$  spectra for the T7.5 GJ 570 D with  $T_{\text{eff}} = 810 \text{ K}$  (Saumon et al. 2006), the T8 2MASS J0415-09 with  $T_{\text{eff}} = 750 \text{ K}$  (Saumon et al. 2007), and the latest-type new UKIDSS dwarf ULAS J0034, whose spectral indices imply a type of T8.5. It can be seen that the H<sub>2</sub>O and CH<sub>4</sub> absorptions in the wings of the *J* and *H* flux peaks form a progressive sequence for these three very late T dwarfs. Warren et al. (in prep.) use synthetic spectra and the well-studied dwarf 2MASS J0415-09 to show that the preferred atmospheric parameters for ULAS J0034 are  $T_{\text{eff}} \approx 650 \text{ K}$  with  $\log g/[m/H]$  of 4.5/0.0 or 5.0/+0.3. The range in age and mass is then 0.5–3 Gyr and 15–30 M<sub>Jupiter</sub>. Hence this dwarf is likely to be younger, less massive and cooler than the previously known coolest T dwarf with well-determined parameters, 2MASS J0415-09, which is aged 3–10 Gyr, has  $T_{\text{eff}}$  725–775 K and mass 33–58 M<sub>Jupiter</sub>.

## 4.4. Identifying the Y Dwarfs

As  $T_{\text{eff}}$  drops below 700 K the K I features should weaken and the absorption bands of NH<sub>3</sub> strengthen; eventually water clouds will form and the near-infrared colors will redden (e.g. Burrows et al. 2003). For practical purposes, the identifying feature for the next, Y, class should lie in the far-red or near-infrared, and should be recognisable at low resolution, as the targets will be faint.

A major problem with predicting the Y dwarf spectral signature is incompleteness in the CH<sub>4</sub> and NH<sub>3</sub> linelists in the red and near-infrared. While laboratory studies and calculations are underway (e.g. Barber et al., these proceedings), the current situation makes line identification in known objects, and predictions for the Y dwarfs, very uncertain. Figure 9 shows a synthetic spectrum for a 600 K brown dwarf, a room-temperature NH<sub>3</sub> gas spectrum, and the observed spectra of the 750 K brown dwarf 2MASS J0415-09 and Saturn. The physical environment of a brown dwarf atmosphere is quite different from that of either Saturn or the laboratory data, and there are no clear indications of NH<sub>3</sub> features in the brown dwarf spectrum. Furthermore, vertical mixing will deplete NH<sub>3</sub> by a factor of  $\sim 10$ . If NH<sub>3</sub> nevertheless becomes the spectral indicator for Y dwarfs, Figure 9 shows that the features in the *H* and *K* bands (Burrows et al. 2003) are not likely to be useful, due to the low flux in those regions and the presence of strong H<sub>2</sub>O features. Instead it seems that the changing shape of the

*Y* band as K I disappears from the photosphere, and NH<sub>3</sub> features in the blue wing of the *Y* band and across the *J* band, may be the best Y dwarf indicators.

## 5. Conclusions

Great advances have been made since the CS13 meeting. *Spitzer* has made studies of brown dwarf mid-infrared spectra possible, for the first time. The data show that dredge-up of CO and N<sub>2</sub> must occur from deeper hotter layers of the atmosphere into the photosphere. Also, more very late T dwarfs have been discovered, and surveys like UKIDSS show promise of finding even cooler dwarfs. It is not clear however what the spectral indicator of Y dwarfs will be, largely due to serious deficiencies in the linelists of CH<sub>4</sub> and NH<sub>3</sub> at  $\lambda < 1.6\mu\text{m}$ .

**Acknowledgments.** UKIDSS is made possible by the UK Infrared Telescope (UKIRT), the University of Cambridge Astronomical Survey Unit and the WFCAM Science Archive at the Royal Observatory Edinburgh. UKIRT is operated by the Joint Astronomy Centre for the UK Particle Physics and Astronomy Research Council (PPARC). Based on data obtained by program GS-2006B-Q-36 at Gemini Observatory, operated by the Association of Universities for Research in Astronomy, Inc., under a cooperative agreement with the NSF on behalf of the Gemini partnership: the National Science Foundation

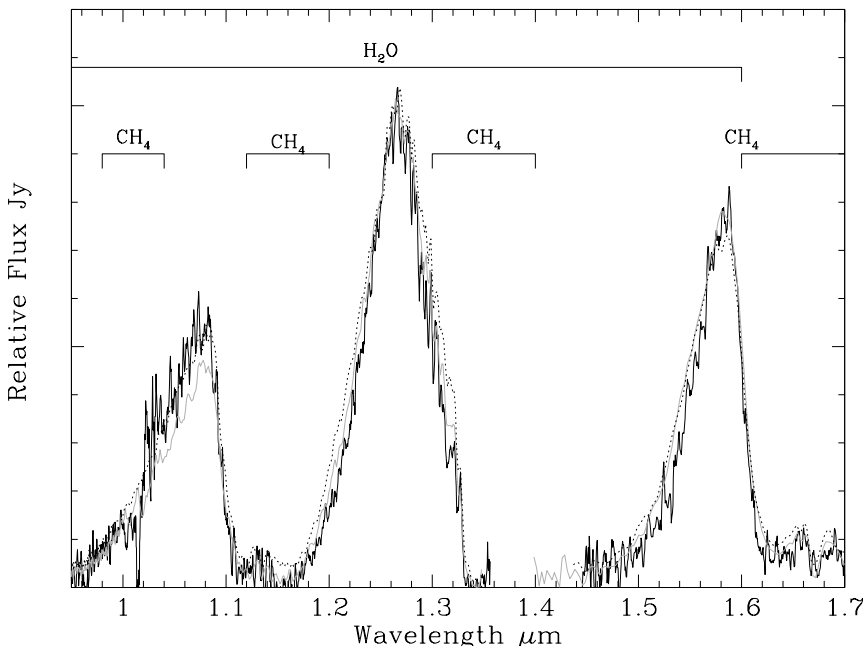


Figure 8. Observed *YJH* spectra of the very late T dwarfs GJ 570 D (dotted curve), 2MASS J0415-09 (grey) and ULAS J0034 (black).

(United States), PPARC (UK), the National Research Council (Canada), CONICYT (Chile), the Australian Research Council (Australia), CNPq (Brazil) and CONICET (Argentina). SL and TG are supported by Gemini Observatory. This work also uses observations made with the *Spitzer Space Telescope*, operated by the Jet Propulsion Laboratory, California Institute of Technology under a contract with NASA. Support was provided by NASA through an award issued by JPL/Caltech. Support also provided under the auspices of the U.S. Department of Energy at Los Alamos National Laboratory by Contract W-7405-ENG-36. MS and DS acknowledge the support of the NASA Office of Space Sciences.

## References

- Ackerman, A. S., & Marley, M. S. 2001, ApJ, 556, 872  
 Becklin, E. E. & Zuckerman, B. 1988, Nature 336, 656  
 Burgasser, A. J., Reid, I. N., Leggett, S. K. et al. 2005, ApJ, 634, L177  
 Burgasser, A. J., Geballe, T. R., Leggett, S. K. et al. 2006a, ApJ, 637, 1067  
 Burgasser, A. J., Kirkpatrick, J. D., Cruz, K. L. et al. 2006b, ApJS, 166, 585  
 Burrows A., Marley, M., Hubbard, W. B. et al. 1997, ApJ, 491, 856  
 Burrows, A., Sudarsky, D., Lunine, J.I., 2003, ApJ, 596, 587  
 Dye, S., Warren, S. J., Hambly, N. C. et al., 2006, MNRAS, 372, 1227

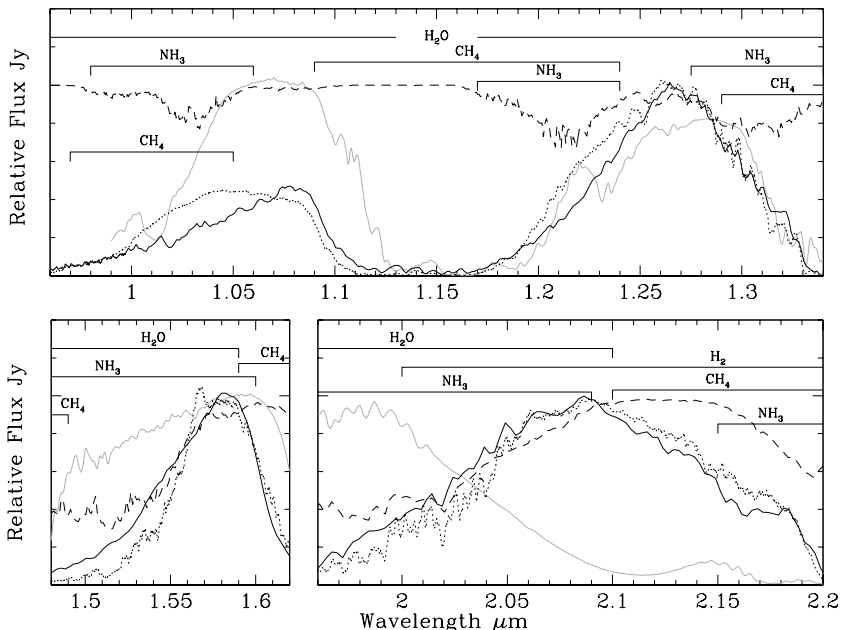


Figure 9. Spectra of the T8 2MASSJ 0415-09 (black curve, Knapp et al. 2004) and Saturn (grey curve, Kim & Geballe 2005). The dotted curve is a  $T_{\text{eff}} = 600$  K synthetic spectrum, and the dashed an  $\text{NH}_3$  absorption spectrum (Irwin et al. 1999).

- Deacon, N. R. & Hambly, N. C. 2006, MNRAS, 371, 1722  
Geballe, T. R., Knapp, G. R., Leggett, S. K. et al. 2002, ApJ, 564, 466  
Golimowski D. A., Leggett, S. K., Marley, M. S. et al. 2004a, AJ, 127, 3516  
Golimowski D. A., Henry, T. J., Krist, J. E. et al. 2004b, AJ, 128, 1733  
Hewett, P. C., Warren, S. J., Leggett, S. K. & Hodgkin, S. T. 2006, MNRAS, 367, 454  
Irwin, P. G. J., Calcutt, S. B., Sihra, K. et al. 1999, JQSRT, 62, 193  
Kendall, T. R., Tamura, M., Tinney, C. G. et al. 2007, A&A, in press  
Kim, S. J. and Geballe, T. R. 2005, Icarus, 179, 449  
Knapp, G. R., Leggett, S. K., Fan, X. et al. 2004, AJ, 127, 3553  
Lawrence, A., Warren, S. J., Almaini, O. et al., 2007, MNRAS, in press  
Leggett, S. K., Saumon, D., Marley, M. S. et al. 2007, ApJ, in press  
Liu, Michael C. & Leggett, S. K. 2005, ApJ, 634, 616  
Luhman, K. L., Patten, B. M., Marengo, M. et al., 2007, ApJ, 654, 570  
Nakajima, T., Oppenheimer, B. R., Kulkarni, S. R. et al. 1995, Nature, 378, 463  
Patten, B. M., Stauffer, J. R., Burrows, A. et al. 2006, ApJ, 651, 502  
Saumon, D., Marley, M. S., Cushing, M. C. et al. 2006, ApJ, 647, 552  
Saumon, D., Marley, M. S., Leggett, S. K. et al. 2007, ApJ, 656, in press  
Skrutskie, M. F., Cutri, R. M., Stiening, R. et al. 2006, AJ, 131, 1163  
Warren, S. J., Hambly, N. C., Dye, S. et al., 2007, MNRAS, in press  
York, D. G., Adelman, J., Anderson, J. E. et al. 2000, AJ, 120, 1579